NONLINEAR STRUCTURAL INSTABILITY OF LONG-SPAN CABLE-STAYED BRIDGES UNDER GRAVITY AND WIND LOADS

By Virote BOONYAPINYO*, Hitoshi YAMADA**, and Toshio MIYATA***

Nonlinear structural instability analyses of a long-span cable-stayed bridge under both gravity loads and displacement-dependent wind loads are presented by finite element approach. The bridge with the center span length of 1000 meters is considered both during erection and on completion. A proposed modeling of structural instability includes the three-component displacement-dependent wind loads as well as all sources of the geometric nonlinearity, such as the beam-column, nonlinear cable, and bridge geometric change. The results show that the long-span cable-stayed bridge is highly geometric nonlinear structure under both gravity and wind loads. This geometric nonlinear and the displacement-dependent wind loads result in significant reduction in the critical wind velocity as well as the instability gravity load. The results also indicate that the partly erected bridge is much more susceptible to the nonlinear lateral-torsional buckling than the completed bridge. Various structural parameters affecting instability load are also investigated.

Key Words: Structural instability, geometric nonlinearity, cable-stayed bridges, gravity and wind loads

1. INTRODUCTION

With the increase in span length of modern cable-stayed bridges, structural stability of the whole bridge under gravity and wind loads presents increasingly important problems both in design and construction. These problems result from the high compressive forces in the towers and deck as well as the large wind-induced forces on the flexible bridge. These problems are of particular importance for long-span cable-stayed bridges using balanced cantilever erection method where the partly erected bridge has much less stiffness than the completed bridge. Under the wind effects, the long-span bridge is subjecte to large, displacement-dependent wind loads of three components, i.e., a drag force, a lift force and a pitching moment. These three-component displacement-dependent wind loads become rapidly large as wind velocity and angle of attack increase, and then may cause lateral-torsion buckling or torsional divergence. In addition, structural instability of long-span cable-stayed bridges is generally preceded by nonlinear load-displacement path because of geometric nonlinearity. This geometric nonlinearity is due to: (1) combined effects of large bending moments and high axial forces in the towers and deck, (2) nonlinear behavior of cable, and (3) bridge geometry change due to large displacements. The nonlinear static behavior of cable-stayed bridges under their own dead loads has been investigated in reference 1, among others.

Previous research on the structural stability of long-span cable-stayed bridges has generally been

* Research Associate, Dept. of Civil Engrg., Yokohama National University, Yokohama 240, Japan.
** Associate Professor, Dept. of Civil Engrg., Yokohama National University, Yokohama 240, Japan.
*** Professor, Dept. of Civil Engrg., Yokohama National University, Yokohama 240, Japan.

based on the linearized buckling analysis under gravity loads [2-7]. The wind-induced structural instability of this type of bridge has also generally been based on the linear method and the separation of three-component wind loads, i.e., the linearized lateral-torsional buckling analysis under the effect of initial drag force, and the torsional divergence analysis under the effect of pitching moment [8-9]. Very few researches, if any, have considered the nonlinear structural instability of this type of bridge under gravity loads and three-component displacement-dependent wind loads.

In this paper, nonlinear structural instability analyses of long-span cable-stayed bridges under both gravity loads and three-component displacement-dependent wind loads are presented by finite element approach. A three-span-continuous cable-stayed bridge with a center span length of 1000 meters and two side spans of 450 meters, in which represents the future trend in design and construction, is considered both during erection and on the completion. The nonlinear structural instability characteristics of this bridge are extensively investigated.

2. METHOD OF NONLINEAR STRUCTURAL INSTABILITY ANALYSIS

2.1 Nonlinear Stiffness Formulation of Bridge Components

A cable-stayed bridge is idealized as an assembly of a finite number of cable and beam-column elements. The nonlinear stiffness formulations of bridge components are summarized in the following subheading. More detail of these formulations can be found in references 1, and 10-12.

(a) Nonlinear stiffness formulation of towers and decks

Tower and deck elements in a cable-stayed bridge are idealized by a three-dimensional beam-column element. The tangent stiffness matrix of the beam-column element consists of the sum of the standard 12 degree-of-freedom elastic stiffness matrix of the beam element and the geometric stiffness matrix of the beam-column element. The geometric stiffness matrix used in this study includes the effects of initial axial force, bending and torsional moments. Therefore, the nonlinear stiffness matrix and various elastic instabilities, such as bending, torsional, and lateral-torsional bucklings, can be considered in the nonlinear instability analysis through this tangent stiffness matrix. The geometric stiffness matrix is given in references 10 through 14.

(b) Nonlinear stiffness formulation of cables

A cable element in a cable-stayed bridge is idealized by a three-dimensional truss element. The nonlinear behavior of cables due to the cable sag is considered through the use of the equivalent modulus of elasticity (or equivalent elastic stiffness) of the cable as an equivalent straight chord element. The tangent stiffness matrix of the cable element is composed of the sum of the elastic stiffness matrix and the geometric stiffness matrix of the truss element. The geometric stiffness matrix is included to consider the large nodal displacements of the stay cable.

2.2 Nonlinear Structural Instability Analysis under Gravity Loads

(a) Incremental equilibrium equation

The structural instability of a long-span cable-stayed bridge is generally preceded by a nonlinear load-displacement path caused by the geometric nonlinearity. Therefore, nonlinear analysis is performed preceding instability analysis to account for the nonlinear prebuckling behavior. In this study, the incremental approach to matrix analysis for nonlinear instability and large displacements is considered. In

the incremental approach, the loads are increased in a series of increments, and in each step the structure is assumed to behave linearly. Beam-column effects are included in an approximate manner through the use of the tangent stiffness matrix, as previously described in subheading 2.1. The nonlinear behavior of cables caused by cable sag is also included through the use of the equivalent cable modulus of elasticity. In addition, the bridge geometry change due to large displacements is taken into account for each step by revising nodal coordinates. Stress computed in a given step are used in the geometric stiffness matrices for both beam-column and cable elements, and are also used in elastic stiffness matrix for cable elements to account for cable sag. The linearized incremental equilibrium equation for the j^{th} step is written as:

$$\left[\mathbf{K}_e\left(u_{j-1}\,,\,\sigma_{j-1}\right)+\mathbf{K}_g\left(u_{j-1}\,,\,\sigma_{j-1}\right)\right]\Delta\mathbf{U}_j = \Delta\mathbf{F}_j \tag{1}$$

where $\mathbf{K}_e$ is the structural stiffness matrix, $\mathbf{K}_g$ is the structural geometric stiffness matrix, $\Delta\mathbf{U}_j$ is the incremental displacement vector, $\Delta\mathbf{F}_j$ is the incremental applied load vector. In Eq. (1) the symbols $\mathbf{K}_e(u_{j-1}, \sigma_{j-1})$ and $\mathbf{K}_g(u_{j-1}, \sigma_{j-1})$ mean that the $\mathbf{K}_e$ and the $\mathbf{K}_g$ are found using both displacements u_{j-1} and the stresses σ_{j-1} from the preceding step.

(b) Automatic load increment strategies

In the incremental approach for nonlinear instability, the proper selection of load increments is necessary to increase the computational efficiency and convergence rate of the problem. Generally, it is of significant advantage to employ large load increments initially and smaller load increments as the instability load is approached. In this study, depending on the response and load level, two different load constraints are considered for the automatic selection of load increments; namely, a constant increment of external work [15] and an eigenvalue analysis. The basic idea of the constant increment of external work is that the nonlinear load-displacement response of a system is correlated to the energy absorption/dissipation process. However, this method may not be effective near the buckling point because at buckling the loads and displacements are in orthogonal directions. Therefore, the eigenvalue analysis is applied near the instability point, while the constant increment of external work is applied in the response far from the instability point.

The incremental load for the j^{th} step is expressed as

$$\Delta\mathbf{F}_j = \Delta\delta_j\,\mathbf{F}_{ref} \tag{2}$$

where $\Delta\delta_j$ is the load incremental parameter for the j^{th} step, $\mathbf{F}_{ref}$ is the reference load vector. The $\Delta\delta_j$ can be determined from the strategies based on the constant increment of external work and/or the eigenvalue analysis as follows.

In the strategies based on the constant increment of external work, the $\Delta\delta_j$ for the j^{th} step can be computed from external work:

$$\left(\Delta\delta_j\,\Delta\mathbf{U}_{j-1}^t\right)\left(\Delta\delta_j\,\mathbf{F}_{ref}\right) = \Delta W_o\,,\ \text{or}\quad \Delta\delta_j = \sqrt{\frac{\Delta W_o}{\Delta\mathbf{U}_{j-1}^t\,\mathbf{F}_{ref}}} \tag{3}$$

where $\Delta W_o = \mathbf{U}_o^t\,\mathbf{F}_{ref}$ is the external work calculated from the first incremental step. It can be seen from Eqs. (2) and (3) that when large displacements occur (corresponding to highly nonlinear response), a small load increment is automatically applied.

In the strategies based on the eigenvalue analysis, the $\Delta\delta_j$ for the j^{th} step can be computed from:

$$\Delta\delta_j = c\,\Delta\lambda \tag{4}$$

where $\Delta\lambda$ is the incremental eigenvalue, as will be introduced later in the next subheading, c is a given constant depending on the distance between the current equilibrium state and instability point.

(c) Computation of instability load factor and mode

The computation of nonlinear instability load factor is conducted in a series of increments using the above automatic load increment strategies. The determination of instability load factor may be found by analysis of the tangent structure stiffness or by eigenvalue analysis. The first method yields the instability load factor and corresponding pattern of displacements. On the other hand, the eigenvalue analysis gives instability mode, in addition to the load factor and displacements.

To calculate the instability mode, the eigenvalue analysis is performed just before the instability. The eigenvalue analysis is performed at initial state and at some incremental steps to measure the distance between the current equilibrium state and instability point. The linearized eigenvalue problem for the j^{th} step is written as:

$$\left[\left\{\mathbf{K}_e(u_{j-1},\ \sigma_{j-1}) + \mathbf{K}_g(u_{j-1},\ \sigma_{j-1})\right\} + \Delta\lambda\,\mathbf{K}_g(u_j,\ \Delta\sigma_j)\right]\Delta\mathbf{U}_j = 0 \tag{5}$$

The computed value $\Delta\lambda$ reduces the effective stiffness of structure to zero with respect to the instability mode. The predicted instability load is

$$F_{cr} = F_{j-1} + \Delta\lambda\,\Delta F_j \tag{6}$$

Eq. (5) assumes that from the j^{th} step onward the elastic and geometric stiffness matrices change proportionally with additional load increments. This assumption becomes more nearly true as F_{j-1} approaches F_{cr}. By using a sequence of increasing load $\mathbf{F}$, one can approach the correct instability load arbitrarily closely. At convergence, $\Delta\lambda = 0$ and $F_{cr} = F_{j-1}$. The eigenvector $\mathbf{U}$ in Eq. (5) describes the buckling mode. If the buckling mode is related to the prebuckling pattern, the neutral equilibrium represents the limit point or, if it is not related, the bifurcation point is obtained.

2.3 Nonlinear Structural Instability Analysis under Displacement-Dependent Wind Loads

(a) Modeling of displacement-dependent wind loads

The three-component displacement-dependent wind loads per unit span acting on the deformed deck can be written in the bridge axes as [10-12] (Fig. 1)

$$F_X(\alpha) = \tfrac{1}{2}\rho V_r^2 A_n C_X(\alpha);\quad F_Y(\alpha) = \tfrac{1}{2}\rho V_r^2 B C_Y(\alpha);\quad M_Z(\alpha) = \tfrac{1}{2}\rho V_r^2 B^2 C_Z(\alpha) \tag{7 a-c}$$

where

$$C_X(\alpha) = \left[C_D(\alpha) - C_L(\alpha)\frac{B}{A_n}\tan\alpha_0\right]\sec\alpha_0;\quad C_Y(\alpha) = \left[C_L(\alpha) + C_D(\alpha)\frac{A_n}{B}\tan\alpha_0\right]\sec\alpha_0;$$
$$C_Z(\alpha) = [C_M(\alpha)]\sec^2\alpha_0;\quad V_r = V\cos\alpha_0 \tag{8 a-d}$$

In Eqs. (7) and (8), F_X, F_Y and M_Z are, respectively, the drag force, lift force, and pitching moment in the bridge axes; C_X, C_Y and C_Z are the static aerodynamic coefficients in the bridge axes; C_D, C_L and C_M are the static aerodynamic coefficients in the wind axes (Fig. 2); V is the mean wind velocity that includes the fluctuation of wind speed on time and space as well as the dynamic amplification; V_r is the relative wind velocity (horizontal component) in bridge axes; ρ is the air density; B is the deck width; A_n is the vertical projected area of deck; α is the effective wind angles of attack consisting of the torsional displacement of

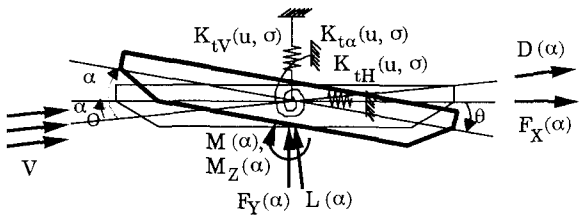

Fig. 1 Motion of a bridge deck and displacement-dependent wind loads in wind and bridge axes

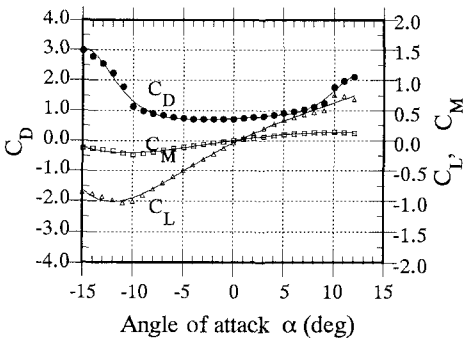

Fig. 2 Static aerodynamic coefficients as a function of angle of attack [16]

deck θ and the wind angle of incidence α_0.

In Fig. 1, D, L, and M are, respectively, the drag force, lift force, and pitching moment in the wind axes. If the wind angle of incidence α_0 is zero, the F_X, F_Y and M_Z are, respectively, equal to D, L and M. Moreover, if the effects of drag and lift forces are neglected in wind load modeling, one obtains the conventional modeling of pitching moment for torsional divergence analysis [12].

(b) Modeling of nonlinear lateral-torsional instability

The modeling of nonlinear buckling under the displacement-dependent wind loads is composed of a two-step process. In the first step process, nonlinear analysis under the initial wind forces of given wind velocity V is performed in one step, utilizing the tangent stiffness of the deformed bridge under dead-load state. In the second step process, nonlinear analysis under the additional wind forces induced by increasing angle of wind attack due to the torsional deformation of the deck is performed. The linearized incremental equilibrium equation of the whole bridge subjected to the additional wind forces for j^{th} iteration is written as

$$\begin{aligned}&\left[\mathbf{K}_e\left(u_{j-1}, \sigma_{j-1}\right) + \mathbf{K}_g^{G+W}\left(u_{j-1}, \sigma_{j-1}\right)\right] \Delta\mathbf{U}_j \\ &= \mathbf{F}_j\left(F_X(\alpha_j), F_Y(\alpha_j), M_Z(\alpha_j)\right) - \mathbf{F}_{j-1}\left(F_X(\alpha_{j-1}), F_Y(\alpha_{j-1}), M_Z(\alpha_{j-1})\right)\end{aligned} \tag{9}$$

where $\mathbf{K}_e$ and $\mathbf{K}_g$ are, respectively, the structural elastic and geometric stiffness matrices based on the displacements u and stresses σ from the preceding iterations; superscripts G and W mean gravity and wind loads, respectively; $\Delta\mathbf{U}_j$ is the incremental displacement vector; $\mathbf{F}_j$ and $\mathbf{F}_{j-1}$ are the displacement-dependent wind load vectors based on the current and preceding wind angles of attack, respectively.

The above process will converge for any given wind velocity less than the critical wind velocity. The convergence criteria for the given wind velocity reaches when the Euclidean norm of static aerodynamic coefficients is less than the prescribed tolerance, i.e.,

$$\left[\sum_{}^{N_a} \left\{C_k(\alpha_j) - C_k(\alpha_{j-1})\right\}^2 \Big/ \sum_{}^{N_a} \left\{C_k(\alpha_{j-1})\right\}^2\right]^{1/2} \le \varepsilon_k, \quad k = X, Y, Z \tag{10}$$

where ε_k represents the prescribed tolerance, N_a = a number of nodes subjected to the displacement-dependent wind loads.

(c) Computation of critical wind velocity

Because the three components of wind loads are a nonlinear function of the angle of wind attack, the procedure for calculation of the critical wind velocity involves the outermost cycle of iteration, in addition to inner cycle of iteration for convergence of each given wind velocity described above. A combination of the eigenvalue analysis with respect to wind forces, i.e., $\left|\left(\mathbf{K}_e + \mathbf{K}_g^G\right) + \lambda \mathbf{K}_g^W\right| = 0$, and the updated wind-velocity bound algorithm is applied to choose the next trial critical wind velocity. This procedure is given in references 10 through 12. The final critical wind velocity reaches when the stable and unstable wind velocities approach to each other.

3. MATHEMATICAL MODELING OF CABLE-STAYED BRIDGES STUDIED

A three-span-continuous steel cable-stayed bridge with a 1000 m center span and two 450 m side spans was investigated for structural instability under both gravity and wind loads. This bridge was designed for representing the future trend in design and construction of the long-span cable-stayed bridge by Hoshino and Miyata [4]. The bridge consists of A-shape towers with 250 m height, an aerodynamic-shape closed-boxed deck with 3 m depth and 39.8 m width including fairing, and double-plane cables. The structural instability analyses were performed for the following combined loads: (1) dead load D (26.5 tf/m); (2) prestresses of cables Ps; (3) live load L (12 tf/m); and (4) wind load W. In the analysis, all the distributed loads are represented by equivalent concentrated joint loads. The static aerodynamic coefficients of the deck are shown in Fig. 2. The nodal displacement-dependent wind loads of three-components were considered for the bridge deck only, while only the initial drag forces were considered for the towers and cables. The fluctuation of wind speed on time and space as well as the dynamic amplification was included

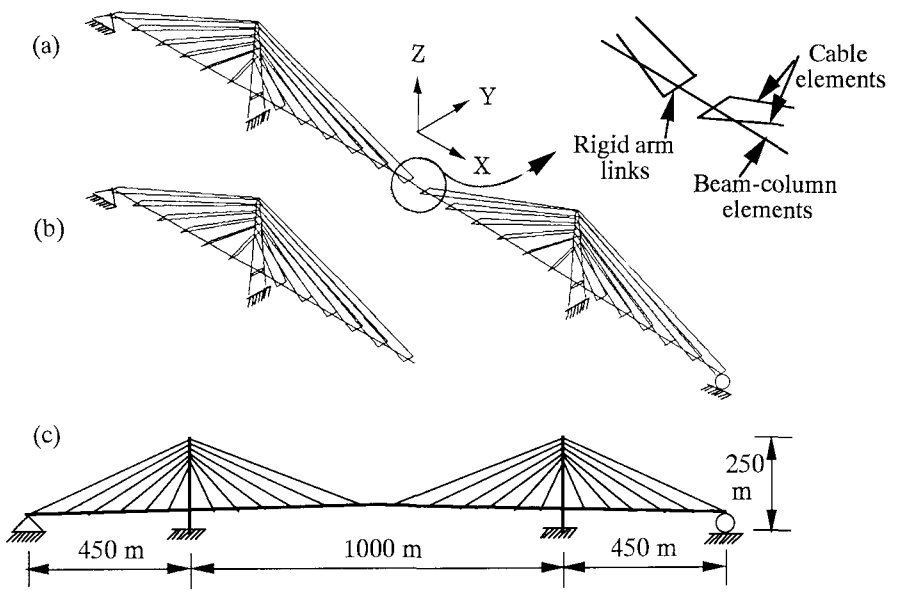

Fig. 3 Finite-element modeling of the studied bridges: (a) a model 1, a 3-D model of the completed bridge; (b) a model 2, a 3-D model of the half-span bridge during erection; and (c) a model 3, a plane model of the completed bridge

in the analysis in an approximate manner through the use of gust response factor given by the Honshu-Shikoku Code [17].

The three-dimensional finite-element modelings of the completed bridge and the half-span bridge just before closing are, respectively, shown in Figs. 3a and 3b; and the plane finite-element modeling is shown in Fig. 3c.

4. STRUCTURAL INSTABILITY CHARACTERISTICS UNDER GRAVITY LOADS

4.1 Structural Parameters Affecting Buckling Characteristics

The structure parameters affecting elastic buckling characteristics of long-span cable-stayed bridge under bridge dead weight and prestresses of cables were investigated by linearized buckling analysis. The plane finite-element bridge model 3 with about 30 percent reduction of the tower stiffness in the longitudinal bridge direction was used in the analysis to compare the buckling mode shapes easily in the structural parametric study.

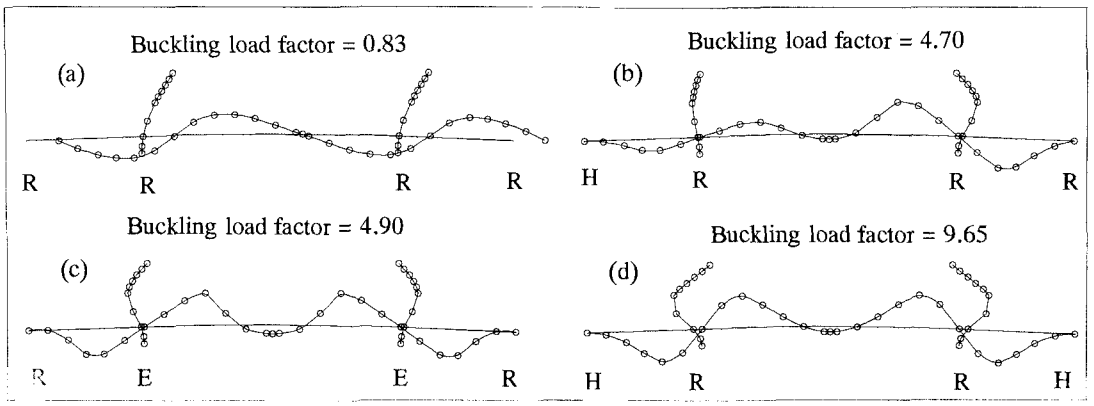

Fig. 4 Effect of longitudinal supports of deck on the buckling load factors and modes for the bridges with four different types of longitudinal supports: (a) without longitudinal restraint; (b) hinge support at one end; (c) longitudinally elastic supports (axial stiffness = 5000 tf/m) at both towers; and (d) hinge supports at both ends; (R=Roller, H=Hinge, E=Elastic)

(a) Effect of longitudinal supports of deck

The elastic buckling load factors and mode shapes for the bridges with four different types of longitudinal support of deck are shown in Fig. 4. The computed buckling load factors are 0.83, 4.70, 4.90, and 9.65 for the bridges with support systems (a), (b), (c) and (d), respectively. It can be seen that the buckling characteristics of the long-span cable-stayed bridges under gravity load are highly dependent on the manner of the longitudinal support of the bridge deck. Small longitudinal restraint results in low buckling load factor and buckling of ohetower, while large longitudinal restraint yields high buckling load factor and buckling of the deck. However, the large longitudinal restraint will attract much higher earthquake and thermal forces. Therefore, it is very important to select the appropriate longitudinal support of the deck for the long-span cable-stayed bridge to improve both buckling and dynamic characteristics.

Two types of longitudinal support of the deck may be applied to the long-span cable-stayed bridge. The first type is hinge support at one end of deck and roller support at the others. The second type is longitudinally elastic support at both towers.

(b) Effect of cable arrangement

The two common types of cable-stayed bridges, namely, semi-fan type (Fig. 3) and fan type, were investigated. The computed buckling load factors are 4.70 for the semi-fan type (Fig. 4b) and 5.57 for the fan type (Fig. 5). The fan type bridge has as much as 16 % more buckling load factor than the semi-fan type bridge. However, the fan type bridge requires more cable length than the semi-fan type bridge and anchorage problem was not considered here. It can be seen that an increase in cable inclination increases the overall elastic stability of the bridge.

In addition, the difference in buckling mode shapes between the two bridge types should be mentioned. The inflection points in the center span of the semi-fan type are caused by higher stiffness of upper cables, which are back anchored at the side supports.

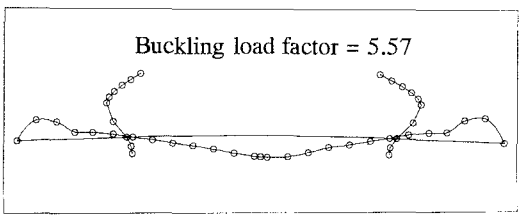

Fig. 5 Buckling characteristics of fan type bridge

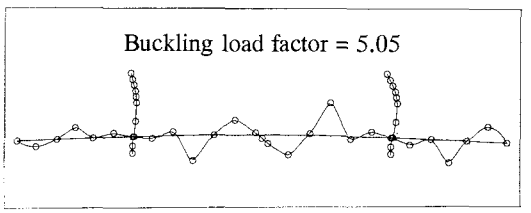

Fig. 6 Buckling characteristics of bridge with two auxiliary supports at side spans

(c) Effect of auxiliary supports at side spans

The bridge with two auxiliary supports at side spans was compared with the bridge without auxiliary supports. The computed buckling load factors are 4.70 for the bridges without auxiliary supports (Fig. 4b) and 5.05 for the bridges with auxiliary supports (Fig. 6). The bridge with auxiliary supports has 7 % more buckling load factor than the bridge without auxiliary supports. It can be seen that the auxiliary supports at side spans increase the overall elastic stability of the bridge.

4.2 Nonlinear Characteristics and Its Instability

The effects of the geometric nonlinearity on the structure characteristics and the buckling load factor were investigated. The geometric nonlinearity, such as beam-column effect, nonlinear behavior of cable and large displacement, was considered both individually and in combination. The plane finite-element bridge model 3, as shown in Fig. 3c, was used in the analysis. All the analyses were performed for the following load sequence: First, the dead load and prestresses were applied in one step, and then the series of live load was applied in increments until instability occurs.

The nonlinear characteristics of the studied bridge described in terms of the load-displacement are, respectively, shown in Figs. 7a and 7b for the vertical displacement of the mid-p of center span and the longitudinal displacement of the left tower top. As can be seen in the figures, the *beam-column* effect and *large displacement* lead to *softening* structure, while the nonlinear behavior of *cables* results in a *hardening* structure. When all sources of geometric nonlinearity are considered, the bridge first exhibits the hardening

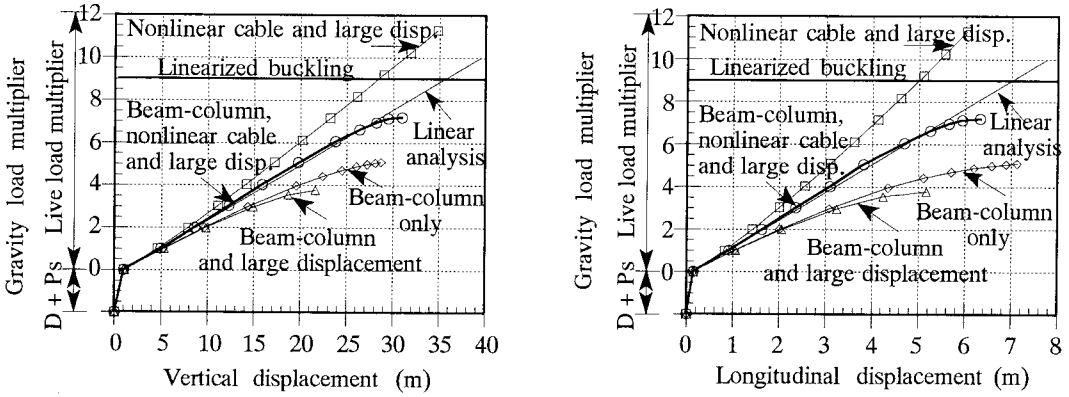

Fig. 7 Nonlinear load-displacement characteristics of bridge model 3 using various sources of nonlinearity: (a) vertical displacement at mid-point of center span; and (b) longitudinal displacement at left tower top

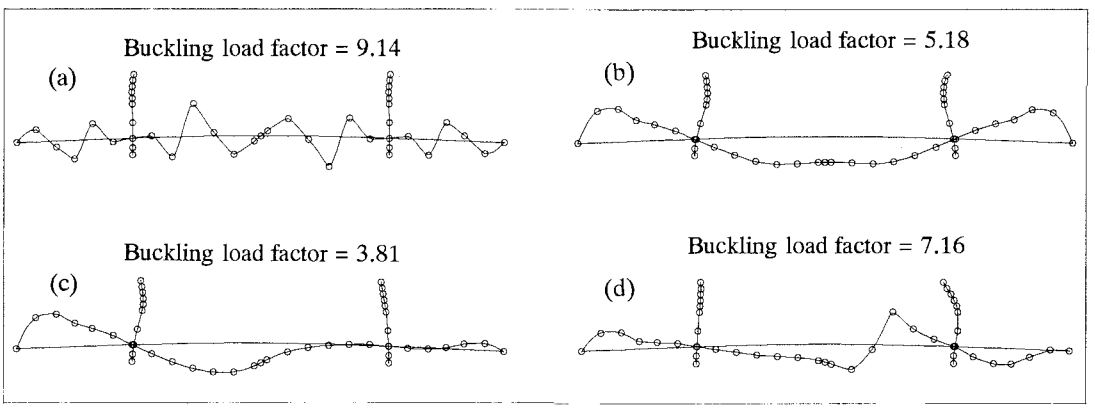

Fig. 8 Buckling mode characteristics of bridge model 3: (a) using linearized buckling analysis; (b)-(d) using nonlinear instability analysis with various sources of nonlinearity; (b) including beam-column effects only; (c) including beam-column effects and large displacement; and (d) including beam-column effects, large displacement and nonlinear cable

structure at the beginning of the incremental load, and then the bridge becomes softening structure as the applied load approaches the buckling load.

The nonlinear instability is also compared with linear instability in Fig. 7. The computed buckling load factors with respect to the live load are, respectively, 9.14 and 7.16 for the linear and nonlinear instability analyses. The buckling load factor obtained from nonlinear instability analysis is as much as 21.7 % lower than that obtained from linear instability analysis. It should be noted that in the past, the buckling load factor obtained form linearized instability analysis is assumed to be conservative because the cables become stiffer under increased loading, as indicated by Tang [2]. However, the results from Fig. 7 indicate that this assumption is not always conservative, particularly for the long-span cable-stayed bridge in which strongly geometric nonlinearity can occur.

The instability mode obtained form linear instability analysis is shown in Fig. 8a, and the instability modes obtained from the nonlinear instability analyses using various sources of geometric nonlinearity are shown in Figs. 8b-8d, in which the buckling modes are described with respect to undeformed bridge geometry. From these figures, the following observations can be made: (1) the linear instability analysis results in both overestimating the buckling load factor and incorrect buckling mode when compared with the results obtained from nonlinear instability analysis; (2) the inflection point of center span in instability mode is caused by the nonlinear behavior of cables (due mainly to geometric stiffness matrix of cable elements and due slightly to increase in equivalent elastic stiffness matrix of cable elements caused by decrease in cable sag).

5. STRUCTURAL INSTABILITY CHARACTERISTICS UNDER WIND LOADS

The three-dimensional finite-element modelings of the completed bridge model 1 shown in Fig. 3a and half-span bridge model 2 just before closing shown in Figs. 3b, were used to investigate the nonlinear structural instability. In this section, nonlinear lateral-torsional buckling characteristics are mainly presented for the partly erected bridges. Nonlinear buckling characteristics of the completed bridges can be found in references 11 and 12. The following loading assumption is made. The bridge dead load and prestresses of the cables are first applied and are kept constant throughout the analysis. Then the displacement-dependent wind loads of three components are simulated and applied on the bridge.

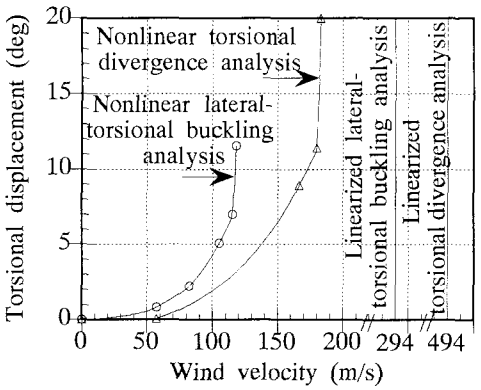

Fig. 9 Torsional behavior at free cantilevering point of half-span bridge model 2 using various instability analysis types

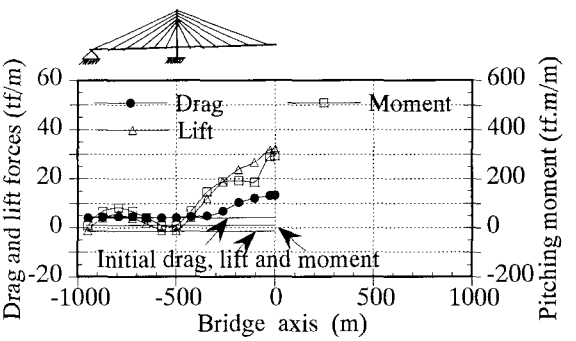

Fig. 10 Three components of displacement-dependent wind loads acting on deck just before instability of half-span bridge model 2 (V_{cr} = 118 m/s, $\theta_{L/2}$ = 11.5 deg)

5.1 Nonlinear Lateral-Torsional Buckling of Partly Erected Bridges

The results of the nonlinear lateral-torsional buckling analysis for the half-span bridge under the displacement-dependent wind loads of three components is shown in Fig. 9. These results show that the nonlinear lateral-torsional buckling analysis results in significant reduction of the critical wind velocity by 60 percent compared with the linearized buckling analysis under the effect of initial wind forces, and by 36 percent compared with the nonlinear torsional divergence analysis under the effect of pitching moment only. The reasons of such a reduction of the critical wind velocity are the considerations of: (a) the increase of the three-component displacement-dependent wind loads due to the torsional displacements of the deck

(Fig. 10), and (b) the relaxation of the equivalent elastic stiffness of the cables due to the effects of lift forces and pitching moments. The critical wind velocity for the lateral-torsional buckling is mainly controlled by the large torsional displacements of the deck (Fig. 9), which in turn increase the three components of wind loads. To reduce the three-component displacement-dependent wind loads, the active aerodynamic control means such as active control surfaces with wings or leading edges may be necessary if the cable-stayed and suspension bridges have much longer span in the future.

The effects of displacement-dependent wind loads and geometric nonlinearity on a buckling mode are shown in Fig. 11 for the half-span bridge. In the linearized buckling analysis, the buckling mode is predominantly a combined vertical bending and torsional mode, together with slightly horizontal mode. However, in the nonlinear buckling analysis, the buckling mode is predominantly horizontal mode. This horizontal mode is probably due to: (1) the low horizontal-bending stiffness of the half-span bridge, and (2) the large lift forces and pitching moments.

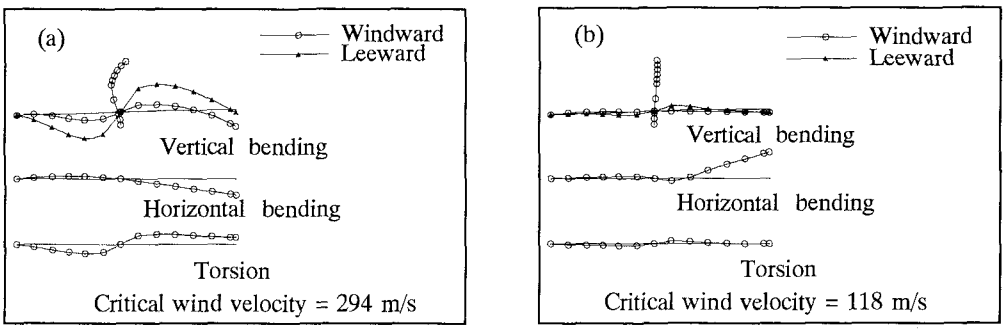

Fig. 11 Effects of displacement-dependent wind loads and geometric nonlinearity on buckling mode and critical wind velocity for half-span bridge model 2: (a) linearized buckling instability; (b) nonlinear buckling instability

5.2 Instability Comparisons between Partly Erected and Completed Bridges

The mid-span torsional and vertical displacement behaviors for the completed bridge and the half-span bridge are shown in Figs. 12a and 12b. The critical wind velocity for the lateral-torsional buckling of the half-span bridge (118 m/s) is 13 percent lower than that of the completed bridge (135 m/s). In addition, the torsional and horizontal displacements of the half-span bridge are much larger than those of the completed bridge. These results clearly show that the half-span bridge is much more susceptible to the nonlinear lateral-torsional buckling than the completed bridge.

5.3 Parametric Study

(a) Erection method

The results of analysis show that the erection method significantly affects the critical wind velocity. In double-side free cantilevering from the tower without temporary supports of bridge deck and tower top, the safety factor against buckling under its own bridge dead load is about to be exhausted. These buckling modes are characterized by one of the following modes: (a) the buckling of the tower having no longitudinal restraint of tower top, and (b) the horizontal buckling of the deck due to the torsional buckling of vertical tower-deck supports. As a result, the critical wind velocity for the lateral-torsional buckling in

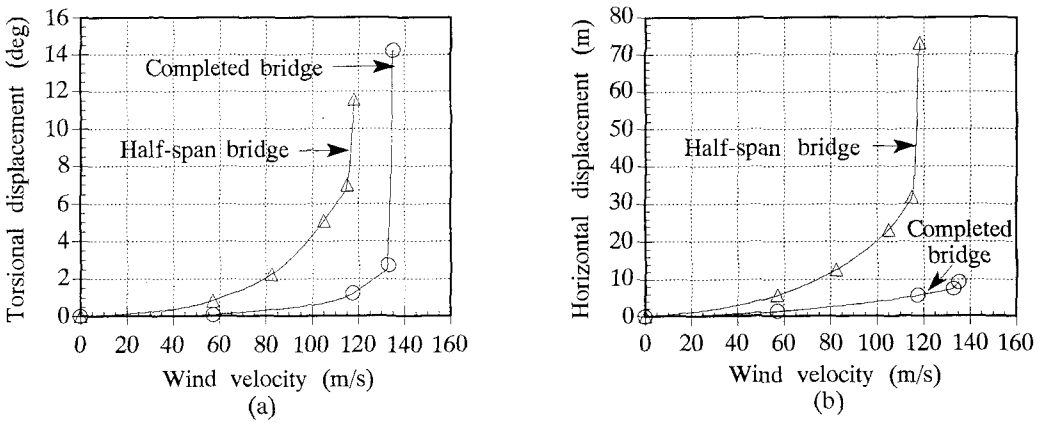

Fig. 12 Comparison of displacement behavior at mid-point of center span between completed bridge model 1 and half-span bridge model 2: (a) torsional displacement; and (b) horizontal displacement

this erection method is relatively low. However, if the two temporary supports of bridge deck at side span as well as one longitudinal support of the bridge deck are provided in double-side free cantilevering method, the critical wind velocities in all processes of erection are much higher than the design one. It can be seen that for the long-span cable-stayed bridge the intermediate supports at side spans are necessary to increase the stability, particularly during erection.

Alternatively, in one-sided free cantilevering of center span with one longitudinal support of the bridge deck, the critical wind velocities for lateral-torsional instability in all processes of erection are much higher than the design one.

(b) Effect of angle of wind incidence

The angle of wind incidence considerably affects the critical wind velocity for both the half-span and completed bridges (Fig. 13). The angle of incidence of + 5 degree (head up) significantly reduces the critical wind velocity from 118 m/s to 90 m/s for the half-span bridge and from 135 m/s to 113 m/s for the completed bridge.

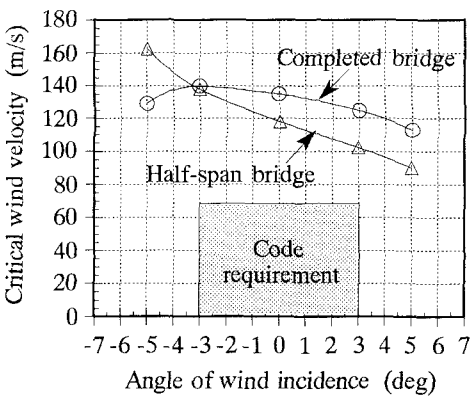

Fig. 13 Critical wind velocities for completed bridge model 1 and half-span bridge model 2 for various angles of incidence

(c) Effect of compressive force contribution to elastic lateral-torsional buckling

The contribution of compressive forces in the deck and towers to the elastic lateral-torsional buckling is largely dependent on the bucking load factor of vertical bending mode under its own dead loads [10]. If this buckling load factor is relatively high (e.g., greater than four times), this compressive force contribution is not significant. This contribution can be simply demonstrated by using the

closed form formula of linear and elastic lateral-torsional buckling for a doubly symmetric beam-column under uniform end moment M and axial force P: $M_{cr} = M_{cro}\sqrt{(1-1/\lambda_b)(1-1/\lambda_t)}$ where Mcr and $Mcro$ are the elastic critical moments in the presence and absence of initial axial force, respectively; λ_b is the bending buckling load factor for the axis normal to the axis of bending; λ_t is the torsional buckling load factor. For the practical cable-stayed bridges, λ_t is very high compared with λ_b, and then λ_t may be neglected.

6. CONCLUSIONS

Nonlinear structural instability analyses of long-span cable-stayed bridges under gravity loads and three-component displacement-dependent wind loads are presented by finite element approach. From the numerical examples of the nonlinear structural instability analysis of the long-span cable-stayed bridge with the center span length of 1000 meters, the conclusions are summarized as follows.

(1) Under gravity loads, the buckling load factor obtained from nonlinear instability analysis is as much as 22 % lower than that obtained from linear instability analysis. This is because the long-span cable-stayed bridge is highly nonlinear structure under gravity loads, where the bridge first exhibits the hardening structure at the beginning of the incremental load, and then the bridge becomes softening structure as the applied load approaches the buckling load.

(2) The incorporation of the three-component displacement-dependent wind loads as well as the geometric nonlinearity in the modeling results in significant reduction in the critical wind velocity, compared with the linearized lateral-torsional buckling modeling under the initial drag force, and torsional divergence modeling under the pitching moment.

(3) The partly erected bridge is much more susceptible to the nonlinear lateral-torsional buckling than the completed bridge. In addition, the erection method significantly affects the critical wind velocity.

Concerning the structural stability under combined gravity and wind loads, the long-span cable-stayed bridge with the center span length of 1000 m presents no serious problem both during erection and on the completion. However, it is expected that the structural instability will present a more crucial mode of failure if a cable-stayed bridge has much longer span in the future.

REFERENCES

1) Nazmy, A. S., and Abdel-Ghaffar, A. M., "Three-Dimensional Nonlinear Static Analysis of Cable-Stayed Bridges," *Computers & Structures*, Vol. 34, No.2, pp. 257-271, 1990.
2) Tang, M. C., "Buckling of cable-stayed girder bridges," *J. of the Structural Division*, ASCE, 102(ST9), pp. 1675-1684, 1976.
3) Gimsing, N. J., *Cable supported bridge: concept and design*, John Wiley and Sons, New York, 1983.
4) Hoshino, M, and Miyata, T., "Design Trial of a Long-Span Cable-Stayed Bridge with Center Span Length of 1000 m.," *Bridge and Foundation Engineering*, Vol. 24(2), pp. 15-22, 1990 (in Japanese).
5) Miyata, T., "Design considerations for wind effects on long-span cable-stayed bridges," *Proc. of the Seminar on Cable-Stayed Bridges: Recent Developments and their Future*, ELSEVIER, Amsterdam, Netherlands, pp. 235-256, 1991.
6) Ito, M., Endo, T., Suzuki, S., and Takagi, N., "Long-span cable-stayed bridge with longitudinally elastic supports," *Structures Congress ' 91 Compact Papers*, ASCE, New York, pp. 506-509, 1991.
7) Endo, T., Iijima, T., Okukawa, A., and Ito, I., "The technical challenge of a long cable-stayed bridge - Tatara Bridge," *Proc. of the Seminar on Cable-Stayed Bridges: Recent Developments and their Future*, ELSEVIER, Amsterdam, Netherlands, pp. 417-436, 1991.

8) Virlogeux, M., "Wind Design and Analysis for the Normandy Bridge", *Proc. of the First Int. Symp. on Aerodynamics of Large Bridges,* Danish Maritime Inst., Copenhagen, Denmark, 1992.
9) Simiu, E., and Scanlan, R.H., *Wind Effects on Structures,* 2nd., John Wiley and Sons, New York, 1986.
10) Boonyapinyo, V., Nonlinear Static Instability Analysis of Long-Span Cable-Stayed Bridges under Gravity and Wind Loads, Doctoral Thesis, Yokohama National University, Yokohama, Japan, 1993.
11) Boonyapinyo, V., Yamada, H., and Miyata, T., "Wind-Induced Nonlinear Lateral-Torsional Buckling of Cable-Stayed Bridges," *J. of Structural Engineering,* ASCE; to appear Feb., 1994.
12 Boonyapinyo, V., Yamada, H., and Miyata, T., "Nonlinear Buckling Instability Analysis of Long-Span Cable-Stayed Bridges under Displacement-Dependent Wind Loads," *J. of Structural Engineering,* JSCE, Vol. 39A, pp. 923-936, March, 1993.
13) Argyris, J. h., Hilpert, O., Malejannakis, G. A., and Scharpf, D. W., "On the Geometric Stiffness of a Beam on a Space-a Consistent Approach," *Computer methods in Applied Mechanics and Engineering,* Vol. 20, pp. 105-131, 1979.
14) Yang, Y. B., and McGuire, W., "Stiffness Matrix for Geometric Nonlinear Analysis, and Joint Rotation and Geometric Nonlinear Analysis," *J. of Structural Engineering,* ASCE, Vol. 112(4), pp. 853-905, 1986.
15) Bathe, K. J., and Dvorkin, E. N., "On the Automatic Solution of Nonlinear Finite Element Equation," *Computers & Structures,* Vol. 17, No. 5-6, pp. 871-879, 1983.
16) Japan Highway Public Corporation, Annual Report 1990 Technical Comm. Meikoh Cable-Stayed Bridge, Japan, 1991.
17) Honshu-Shikoku Bridge Authority, Wind Resistant Design Code for Honshu-Shikoku Bridge, Tokyo, Japan, 1976.

(Received September 16, 1993)